IEEE Access
Multidisciplinary ⋮ Rapid Review ⋮ Open Access Journal

Received March 12, 2020, accepted May 19, 2020, date of publication June 5, 2020, date of current version June 25, 2020.

Digital Object Identifier 10.1109/ACCESS.2020.3000187

A Low-Cost Computational Method for Characterizing Event-Related Potentials for BCI Applications and Beyond

VINICIO CHANGOLUISA[1], PABLO VARONA[2], AND FRANCISCO DE BORJA RODRÍGUEZ[2]

[1]Grupo de Investigación en Electrónica y Telemática, Departamento de Ingeniería en Telecomunicaciones, Universidad Politécnica Salesiana, Quito 170501, Ecuador

[2]Grupo de Neurocomputación Biológica, Departamento de Ingeniería Informática, Escuela Politécnica Superior, Universidad Autónoma de Madrid, 28049 Madrid, Spain

Corresponding authors: Vinicio Changoluisa (fchangoluisa@ups.edu.ec) and Francisco De Borja Rodríguez (f.rodriguez@uam.es)

This work was supported by the Predoctoral Research Grants of the Ecuador Government through of the Secretaría de Educación Superior, Ciencia, Tecnología e Innovación (SENESCYT) under Grant 2015-AR2Q9086, and by the Ministerio de Ciencia, Innovación y Universidades/FEDER under the Spanish Government Grants: TIN2017-84452-R, DPI2015-65833-P and PGC2018-095895-B-I00.

ABSTRACT Event-related potentials (ERPs) are important neurophysiological markers widely used in scientific, medical and engineering contexts. Proper ERP detection contributes to widening the scope of use and, in general, improving functionality. The morphology and latency of ERPs are variable among subject sessions, which complicates their detection. Although variability is an intrinsic feature of neuronal activity, it can be addressed with novel views on ERP detection techniques. In this paper, we propose an agile method for characterizing and thus detecting variable ERPs, which keeps track of their temporal and spatial information through the continuous measurement of the area under the curve in ERP components. We illustrate the usefulness of the proposed ERP characterization for electrode selection in brain-computer interfaces (BCIs) and compare the results with other standard methods. We assess ERP classification for BCI use with Bayesian linear discriminant analysis (BLDA) and cross-validation. We also evaluate performance with both the information transfer rate and BCI utility. The results of our validation tests show that this characterization helps to take advantage of the information on the evolution of positive and negative ERP components and, therefore, to efficiently select electrodes for optimized ERP detection. The proposed method improves the classification accuracy and bitrate of all sets of electrodes analyzed. Furthermore, the method is robust between different day sessions. Our work contributes to the efficient detection of ERPs, manages inter- and intrasubject variability, decreases the computational cost of classic detection methods and contributes to promoting low-cost personalized brain-computer interfaces.

INDEX TERMS Personalized brain-computer interface, brain-machine interface, continuous ERP characterization, event-related potentials, inter- and intrasubject variability, negative ERP, online electrode selection, P300, positive ERP.

I. INTRODUCTION

A brain-computer interface (BCI) is a technology that allows people to communicate with the external environment without relying on the usual peripheral pathways. In recent years, this technology has been widely studied, and modern research has provided different methods to implement it, particularly through event-related potentials (ERPs). However, due to their low speed, long calibration time and low reliability, BCIs are not yet used in daily life tasks [1].

The lack of control of inter- and intrasubject variability is one of the factors that makes it difficult to overcome problems of BCI technology. Additionally, such variable brain responses reflect intrinsic neurophysiological characteristics of the brain and are closely associated with cognitive function varying across individuals, ages, pathological conditions or genetic factors [2]–[5]. Therefore, variability is an intrinsic property of brain function that we must understand and manage.

Currently, ERPs are used to characterize neural variability, and their information can be used to index individual differences in brain function, providing an indicator of variability at the neurophysiological level [5]. For example, changes in ERPs are used as measures for diagnosing neurological and psychiatric diseases. ERPs are also employed in the study of emotions, attention, cognitive processes

The associate editor coordinating the review of this manuscript and approving it for publication was Berdakh Abibullaev.

and personality traits [6]. However, retrieving information from ERPs remains challenging due to the small differences between an ERP and neural background activity. Several methods have been created to improve the performance of ERP-based BCIs. For example, a common approach is a system design that maximizes signal recognition by employing distinct stimulation paradigms to evoke several ERPs [7]–[10]. Another approach is signal processing improvements by optimizing classification algorithms [11]–[13], employing effective methods of selection and extraction of features [14]–[16], or considering electrode selection [17]–[20]. Currently, many of these options involve a high computational cost, and their performance is variable across subjects or sessions [21]–[24]. There is a need for low computational cost methodologies that allow online execution and adaptability between machines and users [1], [22], [25], [26].

In this context, we developed a simple and computationally inexpensive methodology that can characterize the evolution of positive and negative deflections of voltage (a main characteristic of ERPs). This methodology can contribute to subject adaptation and handles variability across sessions, as we discuss below. Our methodology takes advantage of low computational cost measures such as the area under the curve (AUC) applied to the EEG signal, which is widely used and well received in the ERP research community [3], [27]–[29]. In our approach, this measure is continuously calculated and used to characterize positive and negative ERPs throughout the epoch, thus keeping track of their temporal and spatial information. The maximum AUC (*maxAUC*) was calculated as the sum of several AUCs within a sliding window (SW). This SW used in our method covers an entire epoch, considering positive and negative deflections. In this way, we evaluate the existence of ERP features that contribute to the detection of target stimuli. This characterization allows determining more accurately where (electrodes/cerebral lobes) and when (time in ms) ERPs were generated in response to target stimulus.

One direct application of our method of ERP characterization is the selection of electrodes, which can be seen as a feature selection prior to the implementation of any machine learning method. In this paper, we show that the implementation of these methods improves the performance of P300-based BCIs with Bayesian linear discriminant analysis (BLDA). The methodology was tested in a widely used dataset of a P300-based BCI [30] to select the electrodes, i.e., to determine which electrodes provide the best information to the classifier. The proposed ERP characterization method also opens new opportunities to obtain additional information from ERPs beyond the BCI context, as argued in the discussion.

II. MATERIAL AND METHODS

A. ERP VARIABILITY ANALYSIS

To understand the problem we are trying to overcome, it is necessary to mention two facts. (1) Several components are generated after the presentation of a stimulus and not only the ERP that it is intended to evoke. All these components affect the detection of the target stimulus. (2) There is variability in the latency and amplitude of the components in each electrode, among subject sessions and among subjects [3]–[5].

These two issues are present in P300-based BCIs and have been manifested since the seminal paper on BCI by Vidal [31] and later confirmed by several authors [30], [32]–[35]. Variability of amplitude and latency has been described in P300 speller-based BCIs [28] and henceforth shown by several works [32], [36]–[39]. Thus, information useful for the detection of the target stimulus is not concentrated in a specific time interval of an ERP component; rather, it fluctuates during and after the presentation of the stimulus and varies between sessions and subjects.

Both issues can be characterized through a tool widely used in BCIs: Signed-r2-values [32], [40] based on point-biserial correlation, which is a special case of Pearson correlation [41]. This tool measures the association of a continuous variable and a dichotomous variable by providing discriminatory information in the spatiotemporal plane.

In the analysis of ERPs, the continuous EEG signal measured by an electrode is divided into epochs from the onset of the stimulus, and each epoch is labeled as target or nontarget (dichotomous variable). In this study, signed-r2 was implemented in preprocessed EEG signals (as explained in section II-E) under the rapid serial visual presentation (RSVP) model and the oddball paradigm [30]. Each subject underwent four sessions, two on one day (sessions 1-2) and the remaining two on another day (sessions 3-4). This methodology facilitated performing inter- and intrasubject variability analyses.

Figure 1 shows the values of signed-r2 in each subject session. The sequence of ERPs could be seen once the target stimulus was presented. Warm colors represent high values of signed-r2 (positive deflections in the EEG signal), whereas cold colors indicate low values (negative deflections).

The figure shows that discriminant information appears in different brain regions depending on the subject. In some subjects, discriminant information is preserved between sessions of different days, e.g., subject 1 in the electrodes of the frontal and occipital lobes in the range of 335-395 and 540-800 ms or subject 5 in the range of 335-395 ms. In other subjects, it changes from one day to another, e.g., sessions 1-2 in subject 3 present high signed-r2 values between 205 and 325 ms in the frontal lobe and negative values in the occipital lobe. In sessions 3-4 (second day), the maximum values were found in the parietal region in the ranges of 135-195 and 335-410 ms, and negative values were found between 205 and 325 ms in the occipital and parietal (P/O) lobes. Similarly, for subject 8 in sessions 1-2 (first day), the most discriminant information is observed in the P/O in the ranges 155-195 and 285-420 ms; however, in the sessions of the second day, this information appears distributed in all regions.

To corroborate the results of signed-r2, we applied the BLDA classifier throughout the time intervals, which

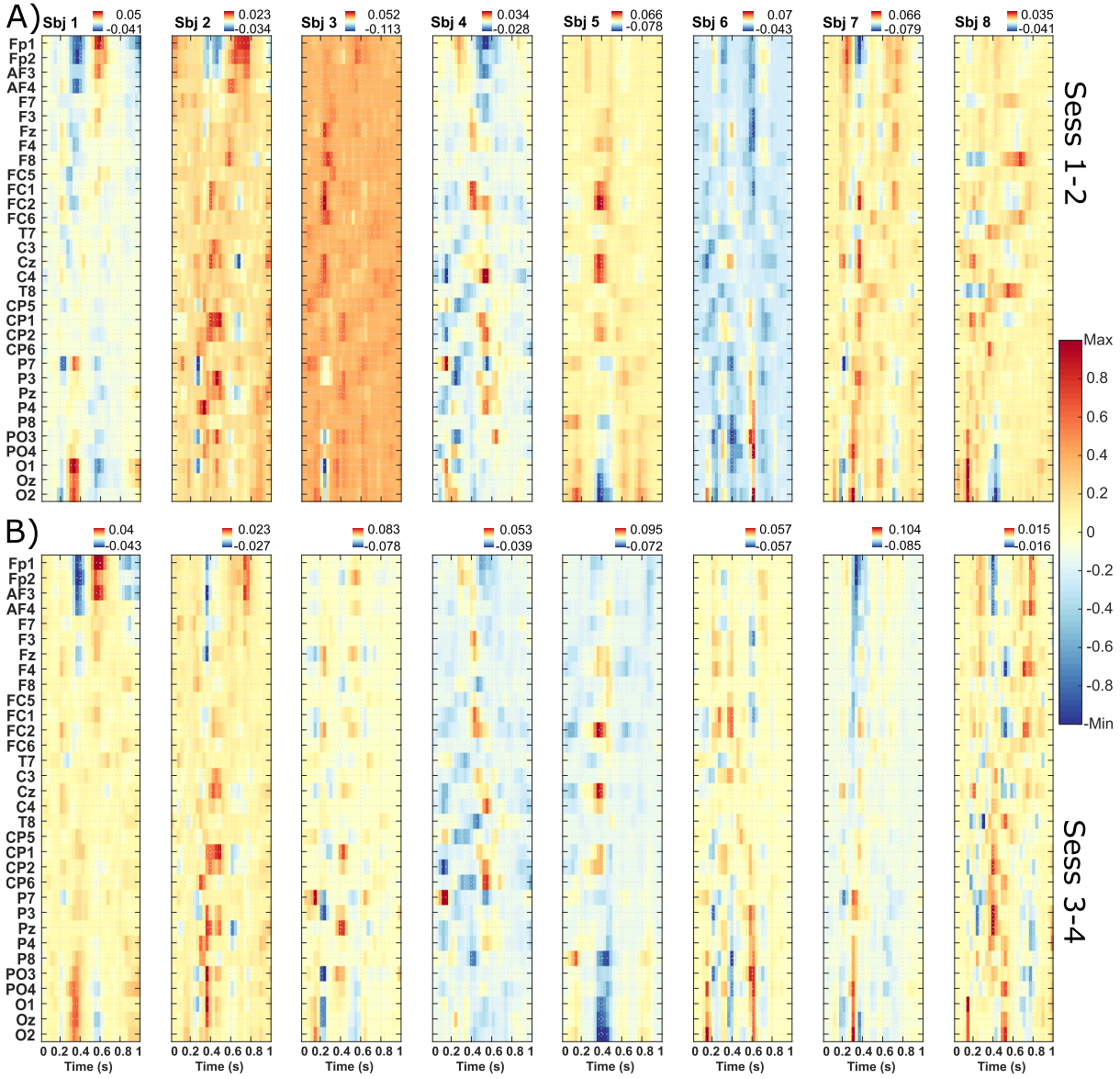

FIGURE 1. Signed-r2 matrix: High values of signed-r2 vary temporally and spatially between subject sessions. Positive and negative ERPs are present at different time intervals at different electrodes. Maximum and minimum values of signed-r2 in each day session are shown in the upper right corner. Panel A) corresponds to sessions 1 and 2 on the first day. Panel B) corresponds to sessions 3 and 4 on another day.

confirmed the separability for detection of the target stimulus. We observed an increase in the accuracy in the time intervals with maximum and minimum values of signed-r2 (see Figure 1 of section 1 in the supplementary information).

In the inter- and intrasubject variability analysis, it is necessary to measure the similarity degree of spatial (i.e., electrodes) and temporal features of events evoked during the presentation of a series of stimuli, in this case under the RSVP model [42], [43]. For this task, cross-correlation was used as a quantitative factor to compare the signed-r2 matrices of the different sessions. We thus measured the degree of similarity between sessions, considering the variability inherent in neuronal activity. This measure shows that the greatest similarity occurs between subject sessions (even when they were recorded on different days), whereas between subjects, there were larger differences. Figure 2 was generated from each session of each subject. A total of 16 matrices (cf. Figure 1) were compared. Warm colors represent the maximum values of similarity between sessions, and cold colors correspond to low similarity.

B. PROPOSED APPROACH: CONTINUOUS ERP CHARACTERIZATION

An ERP is a positive or negative voltage deflection over time. Our method takes advantage of this basic characteristic and continuously measures its evolving AUC. We must highlight that several ERPs may be present in response to a stimulus; for this reason, we calculate the AUC evolution with a sliding window that moves throughout the epoch. In each electrode, this methodology converts EEG signal epochs to a hit vector $\hat{\mathbf{h}}$ considering the stimulation temporal information. This hit

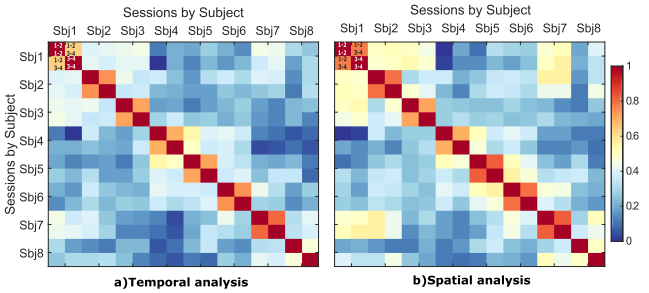

FIGURE 2. **Measure of similarity between sessions per day. Each square represents the cross-correlation between the values of the two signed-r2 matrices (cf. Figure.1) corresponding to sessions 1-2 of one day and 3-4 of another day. The maximum values correspond to the comparison of a session with itself, in warm colors; cold colors represent less similarity. Panel a) represents the comparison between temporal features, and panel b) represents the comparison of spatial features of signed-r2 matrix columns.**

vector characterizes ERPs while maintaining their temporal and spatial features.

To apply the proposed method, the EEG signal of each electrode is divided into epochs and grouped by each set of stimuli presented in a trial; each epoch has an identifier called the stimulus code. For each electrode, we build a 3D matrix $X \in IR^{MxTxQ}$ with M stimulus codes, T samples and Q trials (one trial is equal to a set of M stimuli). To illustrate the application of the *maxAUC* method, let us first consider the MxT matrix of one trial. In each epoch of this matrix, we apply a sliding window (SW) of size n, which can be adjusted according to the duration of the ERP that predominates in the analyzed signal, e.g., around 250 – 300 ms for P300 or around 150 - 200 ms for the N200 ERP [44]. In our application, we apply the two window sizes mentioned above, since they are the most prevalent in ERP-based BCIs [30], [32], [33], [45]–[48]. Therefore, the window size may change depending on each ERP of interest. The SW moved through each sample, from stimulus onset to 1000 ms after.

Within each SW, f subwindows are created, and their AUCs are calculated (see Figure 3); and for this, it is necessary to have an SW with an odd sample size. Then, we choose the central sample to which we add and subtract a sample to obtain a subwindow until reaching the limit of the SW. For instance, if we have an SW of size 7, we obtain 3 subwindows with sizes of 3, 5, and 7 samples. In this way, we seek to give greater advantage to the center of the ERP, which is the one with the greatest amplitude, and therefore, a greater AUC. This procedure is repeated in each M epoch

$$A_{ij} = \sum_{k=1}^{f} AUC(W_{ijk}), \tag{1}$$

where $AUC(W_{ijk})$ is the AUC of the temporal segment W_{ijk} from the ith sliding window of the jth epoch and the kth subwindow. Then, from A_{ij}, we obtain s_i, which is the stimulus code with the highest accumulated AUC for positive deflections.

$$s_i = argmax(A_{ij}). \tag{2}$$

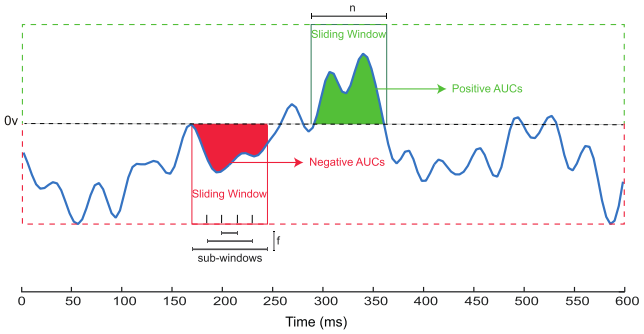

FIGURE 3. **Continuous ERP characterization is achieved progressively by measuring AUC throughout the epoch of the EEG signal, distinguishing positive and negative deflections.**

For negative deflections, we select the stimulus code with the minimum value

$$s_i = argmin(A_{ij}). \tag{3}$$

The hit vector $\hat{\mathbf{h}}$ is built by averaging vectors $\boldsymbol{h}$ as defined as follows: if the stimulus code s_i matches the stimulus code of the target stimulus s_{target}, $h_i = 1$; otherwise, $h_i = 0$:

$$h_i = \begin{cases} 1, & \text{if } s_i == s_{target}, \\ 0, & \text{otherwise.} \end{cases} \tag{4}$$

The component h_i stores the result of each ith sliding window. The average of all vectors $\boldsymbol{h}$ results in the vector $\hat{\mathbf{h}}$, which we call the hit vector; with values between 0 and 1; 1 indicates that in all trials, the stimulus code with maximum AUC corresponds to the stimulus code of the target stimulus, and 0 indicates that it corresponds in no cases. At the end, for each electrode, we obtain two $\hat{\mathbf{h}}$ vectors: one for positive deflections and another for negative deflections. This vector can be seen as a feature vector for multiple further analyses.

C. APPLICATION OF ELECTRODE SCORING

An electrode selection method can use the hit vector $\hat{\mathbf{h}}$ to calculate the score of an electrode. The AUC of each $\hat{\mathbf{h}}$ vector results in a scalar value that represents that score. Although here we used the AUC, other methods can be investigated, i.e., feature selection methods. We illustrate an example of applying this method to P300-based BCI data taken from sessions 3-4 of subject 5 in the dataset [30]. The left panel in Figure 4 shows the EEG signals corresponding to six stimuli: one target (stimulus code 1) and five nontarget stimuli (stimulus code 2-6) in two electrodes: FC2 and O2. Several ERPs are present throughout the epoch. Note the different ERP evolution depending on the electrode. The right panel shows the evolution of the AUC within each SW. This method can be used to characterize positive or negative ERPs by quantifying the positive *maxAUC* (*maxAUC-P*) or negative *maxAUC* (*maxAUC-N*) of the EEG signal.

Figure 5 illustrates how our hit vector characterizes the ERPs present in the EEG signal of each electrode. Panel A shows an average of the EEG signal for each electrode in response to the target stimuli. Several ERPs are present

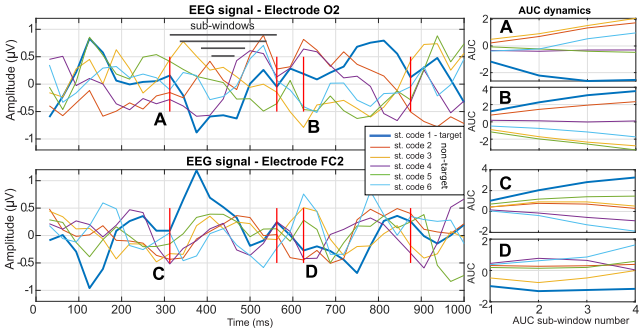

FIGURE 4. **Evolution of the AUC as a function of the stimulus. Positive and negative deflections are present throughout the epoch and vary depending on the electrode. The figure shows the epoch of one target stimulus (dark blue line, stimulus code 1) and five nontarget stimuli per electrode, recorded in electrodes FC2 and O2 (one trial in the same subject). The vertical red lines point out two different intervals of the SW ongoing analysis (beginning at time 312 and 625 ms, respectively). The duration of the SW in this example corresponded to 9 samples, i.e., 281ms. A and D intervals correspond to Negative deflections. B and C intervals correspond to Positive deflections. Left Panels: illustration of the method for the ERPs corresponding to each stimulus. Right panels: AUC values obtained when applying the method. Note that the target stimulus during the SW intervals corresponds to AUC maxima for positive deflections and minima for negative deflections.**

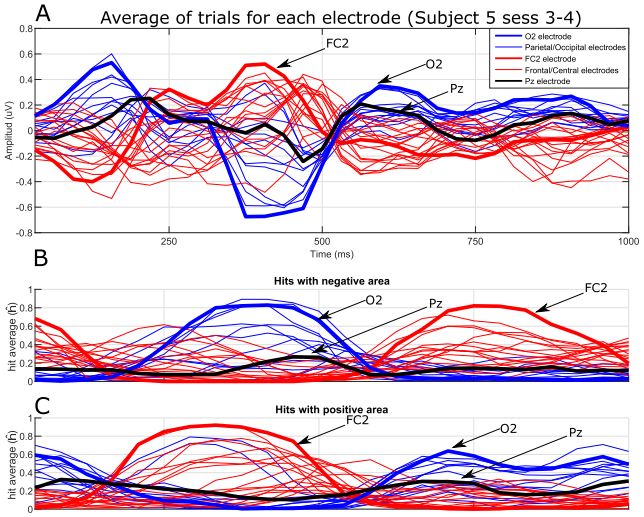

FIGURE 5. **Conversion of a vector of voltage amplitudes to a hit vector. All ERPs throughout an epoch are presented. Panel A: amplitude in time per electrode; in blue, the electrodes of the P/O lobes and in red for the F/C lobes. Panel B: hit vectors for positive AUCs. Panel C: hit vectors for negative AUCs. Each element of a hit vector is the probability that a target stimulus has the maximum (or minimum) amplitude throughout the epoch.**

throughout the epoch and vary in each electrode. The maximum or minimum amplitude is not always found in electrodes that are traditionally used, such as Pz (in black). In fact, they can also appear in other locations, e.g., FC2 or O2, which in some occasions are disregarded, depicted with thick lines. Therefore, this figure shows how these positive and negative deflections of the EEG signal are captured by the *maxAUC* method. In panel A, we can see that between 300 and 500 ms, there are negative deflections in most electrodes located in the P/O lobes, depicted with blue color. These deflections are detected by the *maxAUC* method. In panel B, the value 0.8 out of 1 (80% of trials) reached by electrode O2 represents the percentage of hits in which the minimum AUC in the EEG signal corresponds to a target stimulus. However, we can see that between 200 and 500 ms, there are positive deflections in most electrodes of the frontal and central lobes (F/C), depicted in red. In panel C, it is observed that the *maxAUC* method detects these positive deflections related to the maximum AUC of the target stimulus. In this case, the average hits reach 0.9 out of 1 in electrode FC2.

D. DATASET

We validated the proposed *maxAUC* method in a well-known publicly available database [30]. This dataset contains the data of 4 disabled subjects and 4 healthy subjects. Each subject completed 4 sessions: 2 sessions were performed one day and the remaining 2 sessions were performed another day. Each session had 6 runs, and each run contained data from 32 EEG electrodes placed at the standard positions of the 10-20 international system. Following the oddball paradigm [28], 6 images were presented one by one in random order, and the user was asked to silently count the times that a specific image was repeated. This was called the trial. Each trial was repeated 20 - 25 times per run. Each presentation of an image lasted 100 ms, and during the following 300 ms, no image was presented. For our study of inter- and intrasubject variability, we generated 2 groups of analyses per day: the first group formed sessions 1-2 in one day, and the second group formed sessions 3-4 of another day.

E. PREPROCESSING

For our analysis, before segmenting the signals in epochs, we averaged the signal of two mastoid electrodes that were used as references. The data were filtered with a sixth-order forward-backward butterworth bandpass filter, and cut-off frequencies were set to 1.0 Hz and 12.0 Hz, following previous tests [30]. These data were downsampled from 2,048 Hz to 32 Hz, and each run was standardized to a mean of 0 and standard deviation of 1. For our analysis, we considered an epoch of 1,000 ms from the onset of the stimulus.

F. ELECTRODE SELECTION METHODS

1) TRADITIONAL/STANDARD ELECTRODE SELECTION

In ERP-based BCIs, electrodes located in the occipital and parietal lobes are typically used, as it is assumed that they provide more information and greater precision to detect target stimuli. For example, in the 1970s, Vidal [31] used electrodes of the occipital and parietal lobes: Oz, O1, O2, Pz (10/20 international system) and only one of the frontal lobes, Fz, as an electrode for the artifact detection process. Different electrode combinations between these lobes have been employed, either by increasing the electrodes of the central lobe (Fz, Cz) or those of the posterior lobe (P3, P7, P4 and P8) [30], [49]–[52], the latter significantly increased the accuracy of the detection [30], [32], [33], [45]–[48]. Currently, the standard configuration that mostly uses electrodes located in the parietal and occipital regions and in fewer numbers in the frontal zone is widely accepted, and many authors use it by default [35], [53], [54].

Reference	Year	Electrodes used
Vidal J. [31]	1973	Pz, Oz, O1, O2, Fz
Farwell et al. [28]	1988	Pz
Polikoff et al. [56]	1995	Pz, Cz, Fz
Donchin et al. [49]	2000	Pz, Cz, Fz, O1, O2
Kaper et al. [52]	2004	Pz, Cz, Fz, Oz, P3/4, PO7/8, C3/4
Serby et al. [57]	2005	Pz, Cz, Fz, Oz
Sellers E, Donchin E. [58]	2006	Pz, Cz, Fz
Piccione et al. [59]	2006	Pz, Cz, Fz, Oz
Krusienski et al. [50]	2006	Pz, Cz, Fz, Oz, P3, P4, PO7, PO8
Hoffmann et al. [30]	2008	Pz, Cz, Fz, Oz, P3, P4,P7, P8
Rakotomamonjy et al. [38]*	2008	PO7, PO8
Cecotti et al. [21]*	2011	Pz, Oz, P3, P7, P8
Colwell et al. [17]*	2014	Pz, Cz, Oz, CPz, POz, PO7, PO8
McCann et al. [19]*	2014	Pz, Oz, PO7, PO8
Speier et al. [23]*	2015	CPz, POz, PO7, PO8,
Yu et al. [20]*	2015	Pz, Oz, O1, O2
Ryan et al. [54]	2017	Pz, Cz, Fz, Oz, P3, P4, PO7, PO8
Sheng et al. [35]	2018	Pz, Cz, Fz, Oz, O1, O2
De Venuto et al. [53]	2018	Pz, Cz, P3, P4, CP1, CP2
Guger et al. [60]	2018	Pz, Cz, Fz, C3, C4, CP1, CPz, CP2

* Electrodes selected from an automatic methodology.

TABLE 1. Electrode selection approaches to detect P300-ERPs. Since the first work in P300-based BCIs the Pz electrode has been used in most implementations together with those of the middle line Cz, Fz, Oz. Evidence has shown that the lateral electrodes of P/O lobes also contribute to accuracy improvement of ERP detection.

Another approach is to select the best electrodes according to an automated criterion that scores the information provided in each location. Exhaustive search and greedy search (forward selection and backward elimination methods) stand out [17], [19]–[21], [23], [38], [55]. Although these methods can improve accuracy without a priori information, one of their weaknesses is typically their high computational cost by using exhaustive search or greedy algorithms [19]. Another disadvantage of these methods is their high variability of performance between user sessions, which impacts their generalization performance [19], [21], [23], thus preventing the adaptability of the BCIs. In addition, these methods face the problem of the lack of knowledge regarding what characteristics of the signal are more relevant and best contribute to the accuracy of the BCI. Table 1 chronologically summarizes the evolution of electrode use in P300-based BCIs from the first works in 1973.

In summary, the works discussed above conclude that the electrodes of the central and frontal lobes contain relevant information for ERP-based BCIs and that the posterior lobes contain considerable relevant information for improving the accuracy of this type of BCI [19], [21], [23], [30], [32], [38]. However, when looking for the optimal precision of a BCI, one may want to consider methods of electrode selection adapted to the subject and robust between sessions [21]–[24].

2) PROPOSED ELECTRODE SELECTION CRITERIA

An appropriate personalized selection of the electrodes can lead to an increase in the accuracy of the BCI and a decrease in the computational cost. Systems with few electrodes are easier to configure and more user friendly than systems with many electrodes. It is known that a large set of electrodes does not always increase the precision of the classifier [30]; in fact, in some cases, it is problematic and results in overfitting the model [58], [61]. The challenge, then, is a BCI with few electrodes that achieves high precision.

As we saw in section II-F.1, different electrode configurations have been employed over the years (see Table 1), but all of them maintain in common the presence of the electrode Pz, followed by the electrodes of the midline. Then, lateral electrodes of the posterior part were added, and in some cases, the configuration includes electrodes of the central and frontal lobes. The above described together with the findings of [21] show that although the most relevant electrodes are in the parietal and occipital lobes, the frontal lobe electrodes may also be relevant for some subjects.

With this background, we want to evaluate the evolution of the classifier accuracy as a function of the number and the specific set of electrodes. This evaluation is performed for two kinds of electrode configurations: 1) through the standard electrode selection and 2) by means of the personalized alternative selection proposed in this work based on the AUC and described below.

Our selection of electrodes is based on the electrode score described in section II-C. To select one electrode, we choose the one with the best score. For two or more electrodes, we select one electrode with the highest score from the F/C regions (the one with the highest score), and the remaining electrodes are selected from P/O regions with the highest score (same criterion as in the F/C regions), as illustrated in Figure 6. In this study, in the context of P300-based BCIs, electrodes were selected with the a priori knowledge that there are differences between the components that are generated in different brain lobes [3], [4], [34]. The evidence from several studies that demonstrate improvements in classifier accuracy using electrodes of the posterior brain regions [30], [32], [50], as explained in section II-F.1, were also considered.

Typically, a classification method is used to verify the accuracy of the ERP detection of each set of electrodes. Next, the classification method used in this work is explained.

G. CLASSIFICATION

After the electrodes were selected according to each criterion seen in section II-F, we used their EEG signal for classification. Determining the presence or absence of ERPs is usually considered a binary classification problem. BLDA is a variant of Fisher's LDA [30] and has been widely used in these types of problems with good results [30], [34], [62]. BLDA performs regression in a Bayesian framework that assumes that regression targets t and feature vectors X are linearly related to additive white Gaussian noise n:

$$t = w^T X + n, \tag{5}$$

where w represents the weight vector; with these weights used in regression, we can write the likelihood function. To perform inference in a Bayesian context, it is necessary to specify an a priori distribution, which is defined with a zero-mean Gaussian prior for the weights. These express the penalty, such as the effect of the regularization term used in ridge regression. The posterior distribution can be computed by Bayes' theorem. To obtain the predictive distribution,

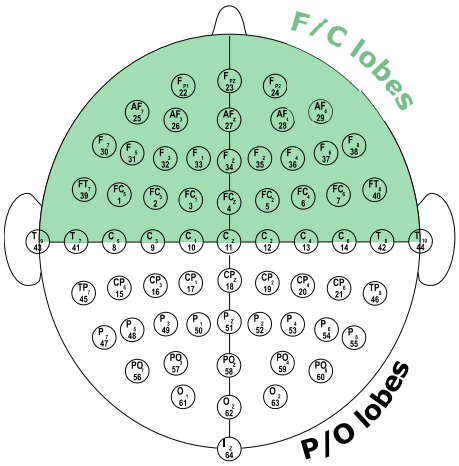

Number of Electrodes	Standard Configuration of Electrodes	Electrodes Selected with the Proposed Method	
		Best Score F/C lobes	Best Score P/O lobes
1	Pz	1 (best score from the 32)	
2	Pz, Cz	1	1
3	Pz, Cz, Fz	1	2
4	Pz, Cz, Fz, Oz	1	3
8	Pz, Cz, Fz, Oz, P7, P3, P4, P8	1	7
10	Pz, Cz, Fz, Oz, P7, P3, P4, P8, C3, C4	1	9

FIGURE 6. Electrode Selection. Electrodes were divided into two groups, one with electrodes from the central and frontal lobes and others from the parietal and occipital lobes (P/O). For the analysis, 6 sets of electrodes were chosen, mostly electrodes with the highest score in the P/O zone, according to the a priori knowledge that more relevant information is found in these lobes (see section II-F.1).

the likelihood function for a new input vector $\widehat{x}$ (i.e., a new epoch to detect the ERP) and the posterior distribution must be multiplied and integrated over w; this distribution was used to obtain the class probabilities by calculating the probability of the target values used during training. The predictive and posterior distributions depend on the hyperparameters α and β. These are calculated by maximizing the likelihood estimation with respect to them through an iterative algorithm described in [63] or [64]. The classifier output is a scalar value, which represents the mean of the predictive distribution of each stimulus. The stimulus with the highest value was considered the target. An expanded version of the classification process can be seen in section 2 of the supplementary information.

H. CROSS-VALIDATION

The classifier was validated using a K-fold cross-validation scheme, where K is equal to two. We trained the model with one session (six runs) and tested it with another (another six runs) and vice versa. This provided two accuracies that were averaged; thus, one subject had an average accuracy per day. Remember that each subject had two sessions per day in two different days (as we saw in section II-D); finally, we obtained 16 accuracies. The accuracy of the classifier was evaluated for each set of electrodes considered in our analysis.

I. STATISTICAL ANALYSIS

The Wilcoxon signed-rank test (WSR test, $p<0.05$) was used to assess whether the difference between the accuracies provided by the *maxAUC-N* method and that of the standard electrode selection was statistically significant.

III. RESULTS

In this section, we show the results of the accuracy achieved with the *maxAUC* method to characterize ERPs and compare the associated performance with the accuracy of electrodes of a widely used standard configuration (see Figure 6). The results show how the *maxAUC* method improves the accuracy of the BLDA classifier when electrodes with better features are selected.

The selected electrodes with the highest score of positive and negative AUCs were tested in the classifier. Throughout the analyses, we used a color code for each set of electrodes. Red indicated the results corresponding to the electrodes with *maxAUC-N*, green indicated those for *maxAUC-P* and black indicated the results for the standard electrodes.

A. MAXAUC ERP DETECTION CONTRIBUTES TO CLASSIFICATION ACCURACY

Figure 7 shows the comparison of the accuracy of six electrode sets. Each panel shows the evolution of the accuracy of 20 trials. The upper left panel shows that a single standard electrode (Pz in all subjects) provided less precision in each trial when compared to an electrode selected for each user with *maxAUC-N* or *maxAUC-P*. This advantage was seen for all sets of electrodes. Better precision was achieved with fewer trials using the *maxAUC* method in each set of electrodes compared.

We show in the same figure that the accuracy of the BLDA classifier with our electrode selection method outperforms the accuracy with the standard electrodes from the first trial. The accuracy of a single selected electrode is comparable to that of three standard electrodes. This advantage over standard electrodes was maintained over all sets of electrodes. Note that the best precision corresponds to electrodes selected with *maxAUC-N*.

With the purpose of making a further quantitative comparison, a measure that we call precision gain P_{gain} was used as a comparative measure of the precision between the *maxAUC* method and the standard electrode sets. P_{gain} is a normalized measure between -1 and 1. Positive values correspond to a better performance of the *maxAUC* method over the use of standard electrodes, whereas negative values correspond to the opposite case. P_{gain} is defined as:

$$P_{gain} = \frac{\sum_{k=1}^{n} \mu_k^{maxAUC} - \mu_k^{std}}{P_p}$$
$$\begin{cases} P_{gain} > 0 & maxAUC \text{ wins}, \\ P_{gain} < 0 & \text{std wins}, \end{cases} \tag{6}$$

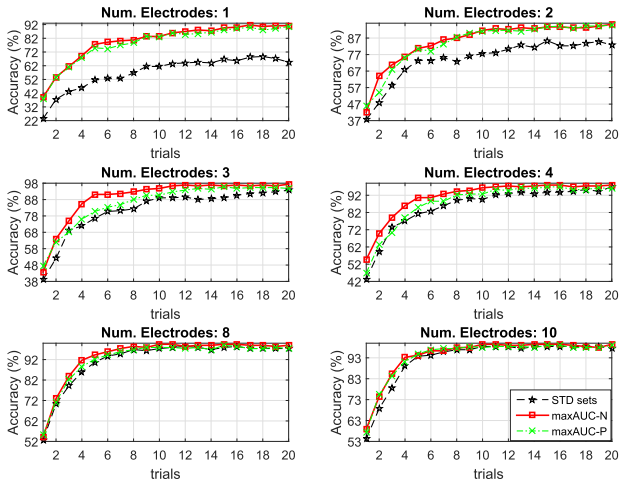

FIGURE 7. **BLDA classifier accuracy by trial for each set of electrodes. From the first trial, the accuracy of the selected electrodes (green and red) was greater than that of the standard set of electrodes (black), described in Figure 6. The accuracy of a single selected electrode was comparable to that of three standard electrodes. Each point represents the average of the 16 accuracy values.**

where μ represents the average accuracy of the 20 trials of the set of electrodes that are being compared, μ^{maxAUC} for the electrode set selected with our methodology and μ^{std} for the standard. P_p is equal to 100%, which represents perfect precision of the classifier, and n is the number of cases to be compared (in our case, $n = 16$). We also measured the percentage in which the *maxAUC* method wins, ties and loses, regarding the standard method, across the obtained 16 accuracies for both methods.

Figure 8 shows a summary of the comparison between electrode sets by day; for this, the 16 accuracies of each set of electrodes were averaged. The accuracy of the electrodes selected with our method was better than that of the standard configuration. The largest difference occurred when few electrodes were used. It is interesting to note that the accuracy of the electrodes selected with *maxAUC-N* surpassed that corresponding to *maxAUC-P*.

Panel A in Figure 8 shows a summary chart of the accuracy achieved with data from first-day sessions. In this panel, we compared the accuracies of *maxAUC-N* and *maxAUC-P* with that of standard electrode sets. The accuracy with one selected electrode surpassed approximately 30% that of the standard electrodes (WSR test, p<0.05). The accuracy of four electrodes selected with the *maxAUC-N* was greater than the accuracy of 10 standard electrodes.

Panel B in Figure 8 shows the P_{gain} calculated with equation (6) and depicts the gain (or loss) of the electrode sets selected with our methodology (described in II-F.2) versus that of the standard electrode configurations currently used. As we mentioned above, positive values indicate that the accuracy of the BLDA classifier achieved with the *maxAUC* method was better than that of the standard electrode configurations. We can see that our method always had an advantage over the standard electrode configurations, and with the configurations of few electrodes,

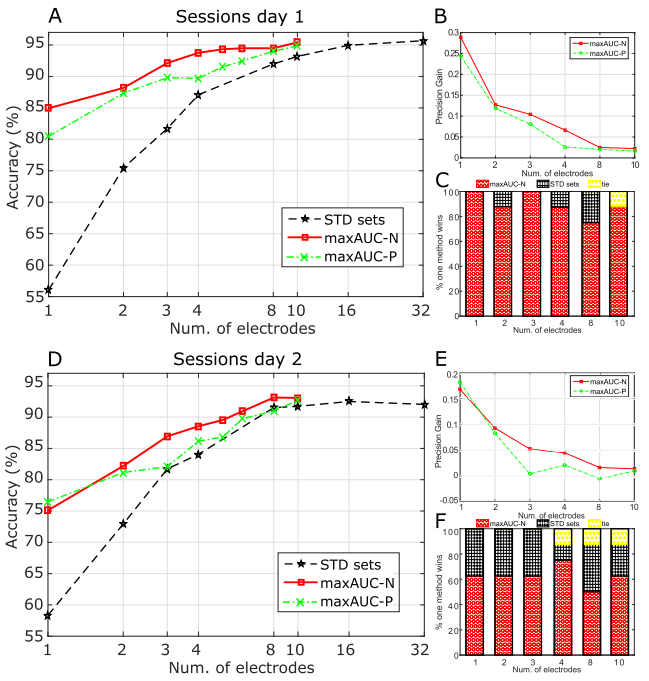

FIGURE 8. **Classifier Accuracy Improvement and Precision Gain. Panel A shows the classifier accuracy of the first-day sessions. Panel B shows a P_{gain} between 1 and -1; 1 when the accuracy of *maxAUC* completely outperforms the standard electrode choice. Panel C (bar graph) shows the percentage of times in which one method outperformed the other, red shows when the *maxAUC* outperforms the standard electrode choice, black corresponds to the opposite case and yellow shows when they match. Panels D, E, and F show the classifier accuracy of the second-day sessions. The accuracy of the electrodes with *maxAUC-N* outperforms all electrode sets compared.**

this advantage was greater. When the number of electrodes increased, the gain in our method decreased, but it was still positive until the configuration of 10 electrodes.

Panel C in Figure 8 depicts the percentage in which the *maxAUC* method wins, ties and loses in each set regarding the standard method. The red color shows how many times our method overcomes the standard electrode choice. The accuracy with one electrode is 100%, i.e., accuracy improves in all sessions for all subjects.

Panels D, E, and F show the accuracy achieved with the data of second-day sessions. Our method maintains an advantage over the standard configuration. The P_{gain} in all electrode sets is better except for the configuration of 8 electrodes in which the difference is minimal with a $P_{gain} = -0.0052$. We also evaluated statistically significant differences in the accuracies of the selected electrodes with *maxAUC-N* and with the standard configuration. Table 2 shows the p-values applying the WSR test. This analysis was performed on each dataset for each day. Values less than 0.05 were obtained for all p-values, which indicates that our electrode selection method provides better results than the standard electrode selection.

B. BITRATE IMPROVEMENT

Another measure of performance in a BCI, in addition to the accuracy used in the previous section, is the information transfer rate (ITR) proposed by Wolpaw *et al.* [65]

	Number of electrodes in each set					
Day	**1**	**2**	**3**	**4**	**8**	**10**
1	5.72×10^{-25}	2.53×10^{-18}	3.89×10^{-18}	1.66×10^{-11}	2.02×10^{-5}	1.49×10^{-5}
2	2.85×10^{-11}	5.06×10^{-7}	1.02×10^{-7}	1.85×10^{-6}	0,0052	0.0124
Cross-Sess	1.56×10^{-13}	6.87×10^{-7}	1.96×10^{-4}	3.98×10^{-6}	0,0129	5.069×10^{-4}

TABLE 2. Statistical analysis for each day sessions and for cross-session. The table displays the p-values of the accuracy difference of the electrode sets analyzed. A p-value<0.05 was considered statistically significant. Each column represents the number of electrode in each set.

in 1998 and widely used to date [66]–[69]. In this section, we show how our method of electrode selection exceeds the performance of the standard selection method using the ITR metric as a comparative measure for both methods. There are also other metrics, such as BCI-utility [70] that are more focused on the user and that contemplate error correction. That is, the objective of this measure is to consider certain measurable benefits for a BCI user through a function that quantifies the user's benefit over time. To promote the generalization of our results, we applied the BCI-utility metric to our method (see Figure 4 of section 4 in the supplementary information). As expected and given by the precision gain that our method has over the standard, for both metrics, the performance of the selected electrodes with the *maxAUC* method has an advantage over the standard approach.

Next, the quantification of ITR is described, and we used the bitrate definition proposed in [65], in which the equations (7) and (8) are used

$$R = log_2 N + P\, log_2 P + (1-P)\, log_2\,[(1-P)/(N-1)], \quad (7)$$

$$ITR(bits/minute) = R\, 60/\tau, \quad (8)$$

where N is the number of classes (or stimuli, 6 in this study), P is the accuracy and τ is the time in seconds for one trial (2,400 ms in this study), see section II-D. The results of our method showed an increase in bitrate in all datasets (see Figure 9). This figure shows that the bitrate achieved with four electrodes selected with *maxAUC-N* is equal to that of 10 standard electrodes. We also calculated the percentage in which the *maxAUC* method wins, ties and loses, c.f. as in section III-A. Figure 9 shows that our method, in red, generally outperforms the bitrate of standard electrodes, and the advantage is greater for cases in which fewer electrodes are used.

C. ADAPTABILITY OF THE MAXAUC METHOD TO INTER- AND INTRASUBJECT VARIABILITY

The effectiveness of this method regarding adaptability can also be addressed. The electrodes selected in one-day sessions can be used in sessions of another day while maintaining superiority over the standard electrode selection and backward elimination method. To test this, the electrodes selected on the first day were used with the second day data. One can observe that the accuracy obtained with the *maxAUC* methodology remains superior to that of the standard electrode selection and the backward elimination method.

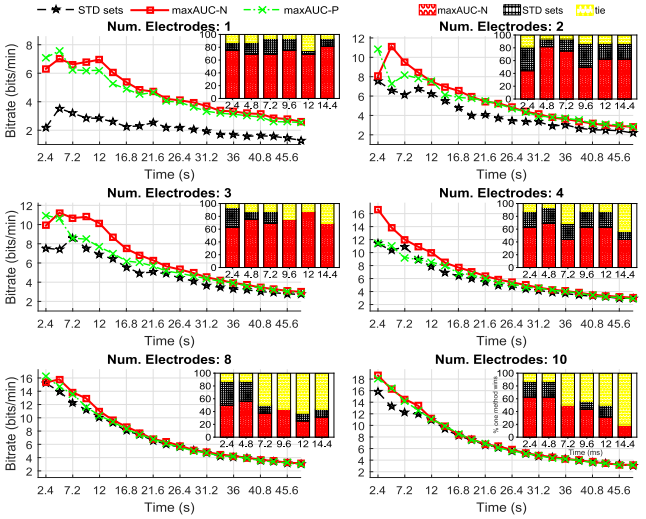

FIGURE 9. Comparison of ITR between standard electrodes and our selection of electrodes. An average of 16 ITR results, two per user. The bar graphs in the upper corner show the times each set outperforms the other, red illustrates when *maxAUC-N* outperforms the standard selection, black corresponds to the opposite case, and yellow shows when they match.

Figure 10 shows three comparative measures. Panel A shows the classifier accuracy of the second-day sessions using the electrodes selected on the first day with our method, the backward elimination method, and the standard electrode selection. The average accuracy of one selected electrode overcomes standard electrode selection by approximately 20%. On average, the sets of 10 selected electrodes reach the highest accuracy, surpassing that of all the standard electrode sets and the backward elimination method. The greatest advantage of the *maxAUC* method with respect to the standard electrode sets is presented when few electrodes are used. Panel B shows the precision gain of each electrode set compared with the standard electrode choice. One can see that *maxAUC-N* outperforms all standard electrode sets. Panel C shows a measure of sensitivity; red depicts the percentage of times that the *maxAUC* method outperforms the standard electrode choice, black indicates the percentage of times that the standard wins and yellow indicates when they tie.

This advantage is also manifested in the statistical analysis, where high levels of statistical significance are obtained, especially for the smaller electrode sets. Table 2 shows the calculated p-values.

In addition to the lack of adaptability of the backward elimination method, its computational cost also impairs its implementation for electrode selection. With backward

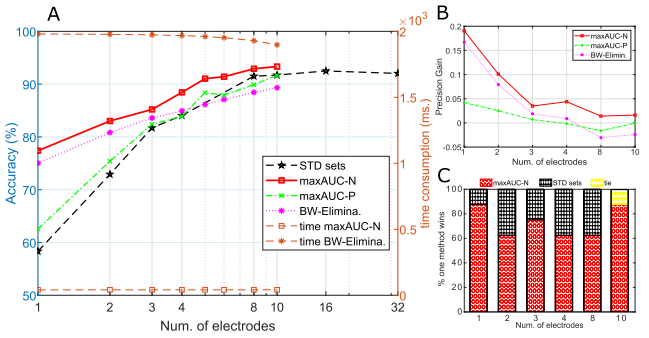

FIGURE 10. **Cross-sessions accuracy summary. Panel A shows the classifier accuracy of the second-day sessions with the electrodes of the first day (left y-axis) and time consumed for the *maxAUC-N* electrodes (mean 41.2795 ms) and the backward elimination electrodes (mean 1,954.9600 ms) (right y-axis). Panel B shows the P_{gain} between 1 and −1; 1 when the accuracies of the *maxAUC* completely outperformed the standard. Panel C (bar graph) shows the percentage of times in which one method outperformed the other, red when *maxAUC* exceeded the standard, black on the contrary and yellow when they matched. The accuracy of the electrodes with *maxAUC-N* outperformed all electrode sets compared.**

elimination, the maximum average accuracy (10 electrodes) of the analyzed electrode sets for the 8 subjects was reached in 1,897.9 ms (1,896.3 ms for electrode selection + 1.69 ms for cross-validation); for the *maxAUC-N* method, the time consumed was 41.53 ms (39.9 ms for electrode selection + 1.63 ms for cross-validation). Figure 10 shows the time consumed for processing the 8 subjects in each set of electrodes. The average time consumed and standard deviation in each set of the *maxAUC-N* electrodes was $41.2795(\pm 0.0987)ms$, and in the backward elimination electrodes, it was $1,954.9600(\pm 28.3515)ms$. This difference in time consumption is because our method performs successive sums to obtain the AUC (numerical integration), which corresponds to linear operations, while backward elimination implements a classification method (SVM, LDA, BLDA, etc.) to select each electrode in each set, which corresponds to nonlinear operations. All experiments were performed on a physical machine with an Intel i7-4790 processor at 3.6 GHz, and 8 GB RAM. The same programming language (MATLAB) and classifier (BLDA) were used for all operations.

The proposed method selects electrodes with their own specific conditions and signal features for each subject session. It was observed that there are electrodes whose selection was repeated for all subject sessions, whereas others changed in each session. Table 3 shows eight electrodes selected in sessions 1-2 of a day and 3-4 of another day for each subject. For all subjects, at least half of the 8 best electrodes of the first sessions (1-2) were repeated in the second (3-4), see the last column of Table 3. The electrodes that were consistently the best in the subject sessions were not necessarily the same among subjects, e.g., subjects 1 and 5 in Table 3.

Finally, we compared our electrode selection methodology with the standard used by Hoffmann *et al.* [30] using the same number of electrodes in each set. Please note that Hoffmann *et al.* did not provide an analysis distinguishing the data on different days. Therefore, we merged the two-day sessions for this comparison. Our electrode sets exceeded the accuracy and ITR with high statistical significance (see Figure 2 and 3 in supplementary information). A detailed description of this analysis can be found in section 3 of the supplementary information.

IV. DISCUSSION

We proposed the use of continuous ERP characterization to improve detection by tracking its temporal evolution. This method characterizes the EEG signal according to positive and negative AUCs over time. The characterization shows that several positive and negative components stand out in an ERP recording. Positive and negative deflections are distributed throughout the poststimulus time and contribute to a better detection of the target stimulus. This approach can serve to select electrodes for BCI applications. The proposed approach can be used in any modern EEG system with a small or large number of electrodes.

The *maxAUC* method characterizes the temporal evolution of ERPs and thus can be implemented in any procedure that involves their detection. The method creates a feature matrix, and each of its rows stores the percentage of times in which the maximum (or minimum) AUCs are related to the target stimulus over time in each electrode. Thus, one of the advantages of this methodology is the characterization in each electrode of the positive and negative deflections that are being generated when a specific stimulus is presented. This could help in identifying specialized brain processes since ERPs are considered electrophysiological markers [5], [71]. In the context of BCIs, our work also benefits those who use a combination of ERPs to improve their accuracy, for example, as in the case of Qin *et al.*, who combined four ERPs P1, N1, P2a, and P2b [47], or Blasco *et al.*, who combined P300 and N2pc [72].

The *maxAUC* electrode selection method simplifies BCI implementation and contributes to improving the associated accuracy. This electrode selection can be understood as a feature selection technique [19], [22], [30], [51], with which we eliminate information redundancy, reduce the number of parameters to optimize the classifier, increase the SNR and identify characteristics related to the targeted neural responses [22]. This approach of selection of electrodes works in three ways by reducing the computational cost, improving the accuracy and contributing to the design of more friendly BCIs through a reduction in the number of electrodes.

The *maxAUC* method allows us to address inter- and intrasubject variability. This variability is caused by functional dynamics in healthy and disabled subjects or by other extrinsic factors affecting electrode conductance, noise, external interference, etc. In the analysis reported in this paper, maximum differences between the signals of target and nontarget stimuli varied among sessions and subjects, as illustrated in Figure 1. By its continuous ERP characterization, the proposed electrode selection method provides improved

Selected Electrodes by Subject										
Sbj	**Sess**	**1**	**2**	**3**	**4**	**5**	**6**	**7**	**8**	**Common Selected Electrodes**
1	**1-2**	PO4	O2	Oz	O1	P3	P7	CP5	Fp1	
	3-4	P8	PO4	Oz	PO3	P3	CP5	CP1	Fp1	Fp1,CP5,P3,Oz,PO4
2	**1-2**	CP2	P4	PO3	Pz	P3	P7	CP1	Fp1	
	3-4	CP6	O1	PO3	P3	P7	CP5	CP1	C3	CP1,P7,P3,PO3
3	**1-2**	O2	O1	PO3	P3	P7	CP5	CP1	FC1	
	3-4	Fp2	PO4	Oz	PO3	Pz	P3	P7	CP1	CP1,P7,P3,PO3
4	**1-2**	FC2	CP6	O2	Pz	P3	P7	CP5	CP1	
	3-4	FC2	CP2	CP6	O2	Oz	O1	P7	CP5	CP5,P7,O2,CP6,FC2
5	**1-2**	CP2	P8	O2	O1	PO3	P3	P7	FC1	
	3-4	FC2	P8	PO4	O2	Oz	O1	PO3	P7	P7,PO3,O1,O2,P8
6	**1-2**	Cz	P8	PO4	O2	PO3	Pz	P3	CP5	
	3-4	P8	PO4	PO3	Pz	P3	CP5	CP1	C3	CP5,P3,Pz,PO3,PO4,P8
7	**1-2**	CP6	P8	PO4	O1	P3	P7	CP5	Fp1	
	3-4	Fp2	CP6	P4	PO4	Oz	P3	P7	CP5	CP5,P7,P3,PO4,CP6
8	**1-2**	T8	P4	PO4	O2	Oz	Pz	P3	CP1	
	3-4	Cz	CP2	O2	Oz	O1	Pz	P3	P7	P3,Pz,Oz,O2

TABLE 3. The electrodes selected with the negative AUC per user sessions are presented. The last column shows the selected electrodes that were common in the two session groups 1-2 and 3-4 in different days. Note that one group of electrodes was the same in the two daily sessions (last column), while the other group changed between sessions. Moreover, it is worth highlighting that for this dataset, the widely used Pz electrode is not selected as the best electrode (see Fig.8, and Fig.10).

classifier accuracy in the detection of target stimuli compared to traditional electrode selection approaches. Another important advantage to this methodology is its robustness between subject sessions. The electrodes selected in the one-day session can be used in the session of another day, maintaining their advantage over standard electrode selection and backward elimination. Negative areas (*maxAUC-N*) are more robust over time than positive areas, see Figure 10, which is in agreement with evidence that shows the importance of the negative deflections in the ERP-based BCIs [23], [30], [32], [51]. Our methodology seems to detect neuronal signatures of visual recognition events evoked during RSVP, manifested in several investigations [42], [43]. However, a deeper study with more sessions of different days is necessary to validate this hypothesis.

When analyzing the variability, we observe that at least 50% of electrodes are again selected between the sessions on different days of each subject. This is consistent with what was previously observed in section II-A , which shows that there is a degree of similarity in spatial information. However, the rest of the electrodes are different, which we attribute to the variation in positions when placing the cap, and the variation in the attentional state of each subject or its environment, which can influence performance, as mentioned in several works [2], [4], [23].

V. CONCLUSION

The proposed method provides efficient detection and continuous characterization of ERPs, manages intersubject variability, decreases the computational cost of classic detection methods and contributes to the search for inexpensive brain-computer interfaces. Furthermore, the method contributes to the design of personalized adaptable BCIs, a challenge that is still latent in this technology. This methodology can also be combined with artifact removal and other methods of feature extraction and/or selection to build further BCI optimizations.

REFERENCES

[1] D. J. McFarland and J. R. Wolpaw, "EEG-based braincomputer interfaces," *Current Opinion Biomed. Eng.*, vol. 4, pp. 194–200, Dec. 2017. [Online]. Available: https://www.sciencedirect.com/science/article/pii/S246845111730082X

[2] J. C. Christensen, J. R. Estepp, G. F. Wilson, and C. A. Russell, "The effects of day-to-day variability of physiological data on operator functional state classification," *NeuroImage*, vol. 59, no. 1, pp. 57–63, Jan. 2012.

[3] S. J. Luck, *An Introduction to the Event-Related Potential Technique*. Cambridge, MA, USA: MIT Press, 2014.

[4] J. Polich, "Updating p300: An integrative theory of P3a and P3b," *Clin. Neurophysiol.*, vol. 118, no. 10, pp. 2128–2148, Oct. 2007.

[5] G. Ouyang, A. Hildebrandt, W. Sommer, and C. Zhou, "Exploiting the intra-subject latency variability from single-trial event-related potentials in the p3 time range: A review and comparative evaluation of methods," *Neurosci. Biobehav. Rev.*, vol. 75, pp. 1–21, Apr. 2017. [Online]. Available: http://www.sciencedirect.com/science/article/pii/S0149763416305590

[6] L. Landa, Z. Krpoun, M. Kolarova, and T. Kasparek, "Event-related Potentials and Their Applications," *Activitas Nervosa Superior*, vol. 56, nos. 1–2, pp. 17–23, Mar. 2014. [Online]. Available: https://link.springer.com/article/10.1007/BF03379603

[7] B. O. Mainsah, G. Reeves, L. M. Collins, and C. S. Throckmorton, "Optimizing the stimulus presentation paradigm design for the P300-based brain-computer interface using performance prediction," *J. Neural Eng.*, vol. 14, no. 4, Aug. 2017, Art. no. 046025. [Online]. Available: http://stacks.iop.org/1741-2552/14/i=4/a=046025

[8] A. Matran-Fernandez and R. Poli, "Brain–computer interfaces for detection and localization of targets in aerial images," *IEEE Trans. Biomed. Eng.*, vol. 64, no. 4, pp. 959–969, Apr. 2017.

[9] S. Zhou, J. Jin, I. Daly, X. Wang, and A. Cichocki, "Optimizing the face paradigm of BCI system by modified mismatch negative paradigm," *Frontiers Neurosci.*, vol. 10, p. 444, Oct. 2016. [Online]. Available: https://www.frontiersin.org/articles/10.3389/fnins.2016.00444/full

[10] E. Yin, T. Zeyl, R. Saab, T. Chau, D. Hu, and Z. Zhou, "A hybrid brain–computer interface based on the fusion of P300 and SSVEP scores," *IEEE Trans. Neural Syst. Rehabil. Eng.*, vol. 23, no. 4, pp. 693–701, Jul. 2015.

[11] A. Barachant and M. Congedo, "A plug&Play P300 BCI using information geometry," 2014, *arXiv:1409.0107*. [Online]. Available: http://arxiv.org/abs/1409.0107

[12] H. Cecotti and A. Graser, "Convolutional neural networks for P300 detection with application to brain-computer interfaces," *IEEE Trans. Pattern Anal. Mach. Intell.*, vol. 33, no. 3, pp. 433–445, Mar. 2011.

[13] D. Hübner, T. Verhoeven, K. Schmid, K.-R. Müller, M. Tangermann, and P.-J. Kindermans, "Learning from label proportions in brain-computer interfaces: Online unsupervised learning with guarantees," *PLoS ONE*, vol. 12, no. 4, Apr. 2017, Art. no. e0175856. [Online]. Available: http://journals.plos.org/plosone/article?id=10.1371/journal.pone.0175856

[14] E. Chiou and S. Puthusserypady, "Spatial filter feature extraction methods for P300 BCI speller: A comparison," in *Proc. IEEE Int. Conf. Syst., Man, Cybern. (SMC)*, Oct. 2016, pp. 003859–003863.
[15] H.-I. Suk and S.-W. Lee, "A novel Bayesian framework for discriminative feature extraction in brain-computer interfaces," *IEEE Trans. Pattern Anal. Mach. Intell.*, vol. 35, no. 2, pp. 286–299, Feb. 2013.
[16] G. Sarasa, A. Granados, and F. B. Rodríguez, "Algorithmic clustering based on string compression to extract P300 structure in EEG signals," *Comput. Methods Programs Biomed.*, vol. 176, pp. 225–235, Jul. 2019.
[17] K. A. Colwell, D. B. Ryan, C. S. Throckmorton, E. W. Sellers, and L. M. Collins, "Channel selection methods for the P300 speller," *J. Neurosci. Methods*, vol. 232, pp. 6–15, Jul. 2014. [Online]. Available: http://www.sciencedirect.com/science/article/pii/S0165027014001253
[18] V. Changoluisa, P. Varona, and F. B. Rodríguez, "An electrode selection approach in P300-based BCIs to address inter-and intra-subject variability," in *Proc. 6th Int. Conf. Brain-Comput. Interface (BCI)*, Jan. 2018, pp. 1–4.
[19] M. T. McCann, D. E. Thompson, Z. H. Syed, and J. E. Huggins, "Electrode subset selection methods for an EEG-based P300 brain-computer interface," *Disab. Rehabil., Assistive Technol.*, vol. 10, no. 3, pp. 216–220, May 2015.
[20] T. Yu, Z. Yu, Z. Gu, and Y. Li, "Grouped automatic relevance determination and its application in channel selection for P300 BCIs," *IEEE Trans. Neural Syst. Rehabil. Eng.*, vol. 23, no. 6, pp. 1068–1077, Nov. 2015.
[21] H. Cecotti, B. Rivet, M. Congedo, C. Jutten, O. Bertrand, E. Maby, and J. Mattout, "A robust sensor-selection method for P300 brain–computer interfaces," *J. Neural Eng.*, vol. 8, no. 1, Feb. 2011, Art. no. 016001. [Online]. Available: http://stacks.iop.org/1741-2552/8/i=1/a=016001
[22] F. Lotte, L. Bougrain, A. Cichocki, M. Clerc, M. Congedo, A. Rakotomamonjy, and F. Yger, "A review of classification algorithms for EEG-based brain–computer interfaces: A 10 year update," *J. Neural Eng.*, vol. 15, no. 3, Jun. 2018, Art. no. 031005.
[23] W. Speier, A. Deshpande, and N. Pouratian, "A method for optimizing EEG electrode number and configuration for signal acquisition in P300 speller systems," *Clin. Neurophysiol.*, vol. 126, no. 6, pp. 1171–1177, Jun. 2015. [Online]. Available: http://www.clinph-journal.com/article/S1388-2457(14)00506-9/abstract
[24] P. Zanini, M. Congedo, C. Jutten, S. Said, and Y. Berthoumieu, "Transfer learning: A Riemannian geometry framework with applications to brain–computer interfaces," *IEEE Trans. Biomed. Eng.*, vol. 65, no. 5, pp. 1107–1116, May 2018.
[25] R. A. Ramadan and A. V. Vasilakos, "Brain computer interface: Control signals review," *Neurocomputing*, vol. 223, pp. 26–44, Feb. 2017.
[26] C. S. Nam, A. Nijholt, and F. Lotte, *Brain–Computer Interfaces Handbook*, 1st ed. Boca Raton, FL, USA: CRC Press, 2018. [Online]. Available: https://www.taylorfrancis.com/books/9781351231947
[27] M. Alvarado-González, E. Garduño, E. Bribiesca, O. Yáñez-Suárez, and V. Medina-Bañuelos, "P300 detection based on EEG shape features," *Comput. Math. Methods Med.*, vol. 2016, pp. 1–14, Jan. 2016.
[28] L. A. Farwell and E. Donchin, "Talking off the top of your head: Toward a mental prosthesis utilizing event-related brain potentials," *Electroencephalogr. Clin. Neurophysiol.*, vol. 70, no. 6, pp. 510–523, Dec. 1988.
[29] V. Changoluisa, P. Varona, and F. B. Rodriguez, "How to reduce classification error in ERP-based BCI: Maximum relative areas as a feature for P300 detection," in *Advances in Computational Intelligence* (Lecture Notes in Computer Science). Cham, Switzerland: Springer, Jun. 2017, pp. 486–497. [Online]. Available: https://link.springer.com/chapter/10.1007/978-3-319-59147-6_42
[30] U. Hoffmann, J.-M. Vesin, T. Ebrahimi, and K. Diserens, "An efficient P300-based brain–computer interface for disabled subjects," *J. Neurosci. Methods*, vol. 167, no. 1, pp. 115–125, Jan. 2008. [Online]. Available: http://www.sciencedirect.com/science/article/pii/S0165027007001094
[31] J. J. Vidal, "Real-time detection of brain events in EEG," *Proc. IEEE*, vol. 65, no. 5, pp. 633–641, May 1977.
[32] B. Blankertz, S. Lemm, M. Treder, S. Haufe, and K.-R. Müller, "Single-trial analysis and classification of ERP components—A tutorial," *NeuroImage*, vol. 56, no. 2, pp. 814–825, May 2011. [Online]. Available: http://www.sciencedirect.com/science/article/pii/S1053811910009067
[33] P. Brunner, S. Joshi, S. Briskin, J. R. Wolpaw, H. Bischof, and G. Schalk, "Does the 'P300' speller depend on eye gaze?" *J. Neural Eng.*, vol. 7, no. 5, Oct. 2010, Art. no. 056013.
[34] H. Cecotti and A. J. Ries, "Best practice for single-trial detection of event-related potentials: Application to brain-computer interfaces," *Int. J. Psychophysiol.*, vol. 111, pp. 156–169, Jan. 2017. [Online]. Available: http://www.sciencedirect.com/science/article/pii/S016787601630633X
[35] Y. Sheng, S. Liu, W. Wang, Y. He, X. Liu, Y. Ke, X. An, and D. Ming, "A study on RSVP paradigm based on brain computer interface across subjects," in *Proc. 9th Int. Conf. Awareness Sci. Technol. (iCAST)*, Sep. 2018, pp. 42–46.
[36] I. Iturrate, R. Chavarriaga, L. Montesano, J. Minguez, and J. Millán, "Latency correction of event-related potentials between different experimental protocols," *J. Neural Eng.*, vol. 11, no. 3, Jun. 2014, Art. no. 036005.
[37] M. R. Mowla, J. E. Huggins, and D. E. Thompson, "Enhancing P300-BCI performance using latency estimation," *Brain-Comput. Interfaces*, vol. 4, no. 3, pp. 137–145, Jul. 2017.
[38] A. Rakotomamonjy and V. Guigue, "BCI competition III: Dataset II-ensemble of SVMs for BCI P300 speller," *IEEE Trans. Biomed. Eng.*, vol. 55, no. 3, pp. 1147–1154, Mar. 2008.
[39] D. E. Thompson, S. Warschausky, and J. E. Huggins, "Classifier-based latency estimation: A novel way to estimate and predict BCI accuracy," *J. Neural Eng.*, vol. 10, no. 1, Feb. 2013, Art. no. 016006.
[40] S.-W. Lee, H. H. Bülthoff, and K.-R. Müller, *Recent Progress in Brain and Cognitive Engineering*. Dordrecht, The Netherlands: Springer, 2015. [Online]. Available: https://link.springer.com/content/pdf/10.1007/978-94-017-7239-6.pdf
[41] R. F. Tate, "Correlation between a discrete and a continuous variable. point-biserial correlation," *Ann. Math. Statist.*, vol. 25, no. 3, pp. 603–607, Sep. 1954.
[42] J. P. Dmochowski, J. J. Ki, P. DeGuzman, P. Sajda, and L. C. Parra, "Extracting multidimensional stimulus-response correlations using hybrid encoding-decoding of neural activity," *NeuroImage*, vol. 180, pp. 134–146, Oct. 2018. [Online]. Available: http://www.sciencedirect.com/science/article/pii/S1053811917304299
[43] A. D. Gerson, L. C. Parra, and P. Sajda, "Cortically coupled computer vision for rapid image search," *IEEE Trans. Neural Syst. Rehabil. Eng.*, vol. 14, no. 2, pp. 174–179, Jun. 2006.
[44] S. H. Patel and P. N. Azzam, "Characterization of N200 and P300: Selected studies of the event-related potential," *Int. J. Med. Sci.*, vol. 2, no. 4, p. 147, 2005.
[45] M. S. Treder and B. Blankertz, "(C)overt attention and visual speller design in an ERP-based brain-computer interface," *Behav. Brain Functions*, vol. 6, no. 1, p. 28, Dec. 2010. [Online]. Available: https://link.springer.com/article/10.1186/1744-9081-6-28
[46] C. Wang, S. Xiong, X. Hu, L. Yao, and J. Zhang, "Combining features from ERP components in single-trial EEG for discriminating four-category visual objects," *J. Neural Eng.*, vol. 9, no. 5, Oct. 2012, Art. no. 056013. [Online]. Available: http://stacks.iop.org/1741-2552/9/i=5/a=056013
[47] Y. Qin, Y. Zhan, C. Wang, J. Zhang, L. Yao, X. Guo, X. Wu, and B. Hu, "Classifying four-category visual objects using multiple ERP components in single-trial ERP," *Cognit. Neurodyn.*, vol. 10, no. 4, pp. 275–285, Aug. 2016. [Online]. Available: https://www.ncbi.nlm.nih.gov/pmc/articles/PMC4947051/
[48] X. Wang, Y. Zeng, Z. Lin, Q. Wu, and B. Yan, "Combining multiple ERP components for detecting targets in remote-sensing images," in *Proc. 9th Int. Conf. Intell. Hum.-Mach. Syst. Cybern. (IHMSC)*, vol. 1, Aug. 2017, pp. 167–170.
[49] E. Donchin, K. M. Spencer, and R. Wijesinghe, "The mental prosthesis: Assessing the speed of a P300-based brain-computer interface," *IEEE Trans. Rehabil. Eng.*, vol. 8, no. 2, pp. 174–179, Jun. 2000.
[50] D. J. Krusienski, E. W. Sellers, F. Cabestaing, S. Bayoudh, D. J. McFarland, T. M. Vaughan, and J. R. Wolpaw, "A comparison of classification techniques for the P300 speller," *J. Neural Eng.*, vol. 3, no. 4, pp. 299–305, Dec. 2006. [Online]. Available: http://www.ncbi.nlm.nih.gov/pubmed/17124334
[51] D. J. Krusienski, E. W. Sellers, D. J. McFarland, T. M. Vaughan, and J. R. Wolpaw, "Toward enhanced P300 speller performance," *J. Neurosci. Methods*, vol. 167, no. 1, pp. 15–21, Jan. 2008.
[52] M. Kaper, P. Meinicke, U. Grossekathoefer, T. Lingner, and H. Ritter, "BCI competition 2003—Data set IIb: Support vector machines for the P300 speller paradigm," *IEEE Trans. Biomed. Eng.*, vol. 51, no. 6, pp. 1073–1076, Jun. 2004.

[53] D. De Venuto, V. F. Annese, and G. Mezzina, "Real-time P300-based BCI in mechatronic control by using a multi-dimensional approach," *IET Softw.*, vol. 12, no. 5, pp. 418–424, Oct. 2018.
[54] D. B. Ryan, G. Townsend, N. A. Gates, K. Colwell, and E. W. Sellers, "Evaluating brain-computer interface performance using color in the P300 checkerboard speller," *Clin. Neurophysiol.*, vol. 128, no. 10, pp. 2050–2057, Oct. 2017.
[55] R. Moro, P. Berger, and M. Bielikova, "Towards adaptive brain-computer interfaces: Improving accuracy of detection of event-related potentials," in *Proc. 12th Int. Workshop Semantic Social Media Adaptation Pers. (SMAP)*, Jul. 2017, pp. 34–39.
[56] J. B. Polikoff, H. T. Bunnell, and W. J. Borkowski, Jr., "Toward a P300-based computer interface," in *Proc. RESNA Annu. Conf. RESNAPRESS Arlington Va*, 1995, pp. 178–180.
[57] H. Serby, E. Yom-Tov, and G. F. Inbar, "An improved P300-based brain-computer interface," *IEEE Trans. Neural Syst. Rehabil. Eng.*, vol. 13, no. 1, pp. 89–98, Mar. 2005.
[58] E. W. Sellers and E. Donchin, "A P300-based brain–computer interface: Initial tests by ALS patients," *Clin. Neurophysiol.*, vol. 117, no. 3, pp. 538–548, Mar. 2006.
[59] F. Piccione, F. Giorgi, P. Tonin, K. Priftis, S. Giove, S. Silvoni, G. Palmas, and F. Beverina, "P300-based brain computer interface: Reliability and performance in healthy and paralysed participants," *Clin. Neurophysiol.*, vol. 117, no. 3, pp. 531–537, Mar. 2006.
[60] C. Guger, R. Spataro, F. Pellas, B. Z. Allison, A. Heilinger, R. Ortner, W. Cho, R. Xu, V. La Bella, G. Edlinger, J. Annen, G. Mandalá, C. Chatelle, and S. Laureys, "Assessing command-following and communication with vibro-tactile P300 brain-computer interface tools in patients with unresponsive wakefulness syndrome," *Frontiers Neurosci.*, vol. 12, p. 423, Jun. 2018.
[61] M. Bittencourt-Villalpando and N. M. Maurits, "Stimuli and feature extraction algorithms for brain-computer interfaces: A systematic comparison," *IEEE Trans. Neural Syst. Rehabil. Eng.*, vol. 26, no. 9, pp. 1669–1679, Sep. 2018.
[62] S. A. Ludwig and J. Kong, "Investigation of different classifiers and channel configurations of a mobile P300-based brain–computer interface," *Med. Biol. Eng. Comput.*, vol. 55, no. 12, pp. 2143–2154, May 2017. [Online]. Available: https://link.springer.com/article/10.1007/s11517-017-1658-2
[63] D. J. C. MacKay, "Bayesian interpolation," *Neural Comput.*, vol. 4, no. 3, pp. 415–447, May 1992.
[64] C. M. Bishop, *Pattern Recognition and Machine Learning* (Information Science and Statistics). Berlin, Germany: Springer-Verlag, 2006.
[65] J. R. Wolpaw, H. Ramoser, D. J. McFarland, and G. Pfurtscheller, "EEG-based communication: Improved accuracy by response verification," *IEEE Trans. Rehabil. Eng.*, vol. 6, no. 3, pp. 326–333, Sep. 1998.
[66] J. M. Egan, G. M. Loughnane, H. Fletcher, E. Meade, and E. C. Lalor, "A gaze independent hybrid-BCI based on visual spatial attention," *J. Neural Eng.*, vol. 14, no. 4, Aug. 2017, Art. no. 046006.
[67] Z. Lin, C. Zhang, Y. Zeng, L. Tong, and B. Yan, "A novel P300 BCI speller based on the triple RSVP paradigm," *Sci. Rep.*, vol. 8, no. 1, p. 3350, Dec. 2018.
[68] M. R. Jones and E. W. Sellers, "Faces, locations, and tools: A proposed two-stimulus P300 brain computer interface," *J. Neural Eng.*, vol. 16, no. 3, Jun. 2019, Art. no. 036026.
[69] N. Zhang, Z. Zhou, Y. Liu, E. Yin, J. Jiang, and D. Hu, "A novel single-character visual BCI paradigm with multiple active cognitive tasks," *IEEE Trans. Biomed. Eng.*, vol. 66, no. 11, pp. 3119–3128, Nov. 2019.
[70] B. Dal Seno, M. Matteucci, and L. T. Mainardi, "The utility metric: A novel method to assess the overall performance of discrete brain–computer interfaces," *IEEE Trans. Neural Syst. Rehabil. Eng.*, vol. 18, no. 1, pp. 20–28, Feb. 2010.
[71] M. Eimer, "Effects of face inversion on the structural encoding and recognition of faces: Evidence from event-related brain potentials," *Cognit. Brain Res.*, vol. 10, no. 1, pp. 145–158, Sep. 2000. [Online]. Available: http://www.sciencedirect.com/science/article/pii/S0926641000000380
[72] J. L. S. Blasco, E. Iáñez, A. Úbeda, and J. M. Azorín, "Visual evoked potential-based brain–machine interface applications to assist disabled people," *Expert Syst. Appl.*, vol. 39, no. 9, pp. 7908–7918, Jul. 2012.

VINICIO CHANGOLUISA received the M.S. degree in bioengineering and telemedicine from the Universidad Politécnica de Madrid, in 2011. He is currently pursuing the Ph.D. degree in informatics and telecommunications with the Universidad Autónoma de Madrid. He was a Visiting Scholar with the Swartz Center for Computational Neuroscience, University of San Diego. He is currently a Professor with the Departamento de Ingeniería en Telecomunicaciones, Universidad Politécnica Salesiana. His research interests include different topics in brain–computer interface, artificial intelligence, and computational neuroscience.

PABLO VARONA received the degree in theoretical physics and the Ph.D. degree in computer science from the Universidad Autónoma de Madrid, in 1992 and 1997, respectively. He held a postdoctoral position and was an Assistant Research Scientist with the Institute for Nonlinear Science, University of California at San Diego. He is currently a Professor of computer science with the Universidad Autónoma de Madrid. His main research interests include computational neuroscience, biomedical engineering, and bio-inspired robotics and devices.

FRANCISCO DE BORJA RODRÍGUEZ received the degree in applied physics and the Ph.D. degree in computer science from the Universidad Autónoma de Madrid, Madrid, Spain, in 1992 and 1999, respectively. He worked at the Instituto de ingeniería del conocimiento (UAM), until 1995. He worked at the Nijmegen University, Holland, Institute for Nonlinear Science, University of California San Diego, Centro de Neurociencias Integradas (CENI) in Santiago de Chile and at Instituto de Física de São Carlos in Universidad de São Paulo (IFSC, USP). Since 2002, he has been a Professor Titular with the Escuela Politécnica Superior, UAM. His areas of interest in investigation are computational neuroscience-chemical sensing-artificial neural networks-biologically inspired robotics-biomedical engineering-information theory and clustering-cryptographic protocols in anonymity.